In Proceedings of the 8th IEEE International Symposium on Biomedical Imaging: From Nano to Macro, ISBI 2011, 361-364, March 30 - April 2, 2011, Chicago, Illinois, USA

MANA – MULTI SCALE ADAPTIVE NORMALIZED AVERAGING

Thobias Romu[1,2,3] *Magnus Borga*[2,3] *Olof Dahlqvist Leinhard*[1,3,4]

[1] Dept of Radiation Physics, CKOC, University Hospital of Linkoping, Sweden. [2] Dept of Biomedical Engineering, [3] Center for Medical Image Science and Visualization (CMIV), [4] Dept of Radiation Physics, IMH, University of Linkoping, Sweden.

ABSTRACT

It is possible to correct intensity inhomogeneity in fat–water Magnetic Resonance Imaging (MRI) by estimating a bias field based on the observed intensities of voxels classified as the pure adipose tissue [1]. The same procedure can also be used to quantify fat volume and its distribution [2] which opens up for new medical applications.

The bias field estimation method has to be robust since pure fat voxels are irregularly located and the density varies greatly within and between image volumes. This paper introduces Multi scale Adaptive Normalized Average (MANA) that solves this problem by basing the estimate on a scale space of weighted averages. By using the local certainty of the data MANA preserves details where the local data certainty is high and provides realistic values in sparse areas.

Index Terms— Image Enhancement/methods, Interpolation, Magnetic Resonance Imaging/methods, Irregularly Sampled Data, Artifacts, Algorithms

1. INTRODUCTION

Sparse and irregularly sampled data are common within different fields such as medical imaging, geology and meteorology but analysis and visualization often require the data to be interpolated or fitted onto a regular grid.

One example is intensity inhomogeneity correction of fat–water Magnetic Resonance (MR) images. The inhomogeneities occur due to changes in the the magnetic field strength and other factors such as variations in coil sensitivity. These errors can be corrected for by observing that pure fat voxels should have the same intensity, independent of location, and then estimating a bias field based on the observed intensities [1]. Pure fat voxels are classified based on the intensity of the fat voxel relative to the sum of the fat and water voxels. The correction is performed using eq. 1.

$$\text{corrected image} = \frac{\text{original image}}{\text{bias field}} \tag{1}$$

After correction of the bias field and a normalization such that pure fat voxels have a unit value, the total amount of adipose tissue within a certain region of interest (ROI) can be estimated by integration within the ROI in the fat image [2]. In this way, estimation errors caused by partial volume effects are avoided and deposits such as bone marrow and subcutaneous, visceral and brown adipose tissue can be quantified separately. This provides an advantage over traditional densitometric methods which estimates the total fat volume based on body volume and weight. The accuracy of the fat quantification by integration is limited by the bias field estimate.

Pure fat voxels will in general be found in unevenly spaced clusters due to the natural distribution of fat in the body. The pure fat voxel density will also vary greatly between individuals as well as location. This means that the method used for estimating the bias field cannot be sensitive to clusters or the distribution of these in the volume. The signal can also be expected to be noisy so interpolation methods that passes through every known data point should be avoided.

The bias field can be estimated by local weighted averages of fat intensities using Normalized Averaging (NA), which can be implemented as a special case of Normalized Convolution (NC) [3]. The locality of the estimate must however be set so that all areas of the volume can be estimated. I.e. the filter applicability must be large enough to cover the largest possible empty region in the data. This disables the possibility of capturing fast changes in information dense areas. Such fast changes are expected in the subcutaneous fat close to coils and due to the tissue–air interface. Since information is dense in these areas an adaptive approach such as Adaptive Normalized Convolution (ANC) [4, 5] is preferable. In this way a local estimate can be made where the differences are expected to be the largest. The drawback is a significant increase in computational complexity, a factor that becomes more important in higher dimensions.

Multi scale Adaptive Normalized Averaging (MANA) provides an adaptive framework for NA much like ANC but with a lower computational complexity. This is accomplished by basing the final estimate on a scale of estimates space using a series of local NA operations on multiple resolutions of the data. In this way the estimate can be made local in dense areas and non local in sparse areas by choosing the appropriate scale for the target voxel.

2. NORMALIZED AVERAGING

NC working on the data s with the constant basis vector $\mathbf{1}$ results in NA. NA constructs local weighted averages for every point. The weights are based on the certainty c of the data and applicability function a of the filter. This operation can be reduced to two convolutions, see eq. 2 where $\cdot$ denotes point wise multiplication.

$$\tilde{s} = \frac{(s \cdot c) * a}{c * a} \tag{2}$$

In the case of NA, the applicability function corresponds to a lowpass filter kernel and will thus be referred to as the kernel for the remainder of this paper.

3. MULTI SCALE ADAPTIVE NORMALIZED AVERAGING

MANA is based on the same operation as NA but builds up a scale space of $s \cdot c$ and c. This is done by repeated downsampling–convolution–interpolation operations. The estimated data $\tilde{s}$ is successively updated for each iteration.

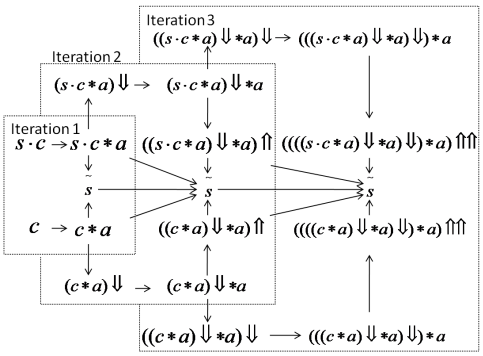

Fig. 1: Illustration of the information flow during the fist three iterations of MANA. Convolutions are indicated by $*$, downsampling by a factor Δ by $\Downarrow$ and interpolation by a factor Δ by $\Uparrow$.

Section 3.1 describes how the operations above creates a scale space and how the result from one iteration is equal to a single convolution of the original data with a gaussian kernel. How the scales are weighted into the final estimation is described in section 3.2.

3.1. Scale Space Creation

One of the central parts of MANA is the downsampling of the data for each iteration. This means that a small gaussian kernel can be used on less and less data to reduce the computational cost. This section presents the general case when different gaussian kernels and downsampling factors are used to create a new scale in each iteration. C denotes the covariance matrix, N the dimensionality and i indexes iterations.

It is well known that a convolution between two gaussians result in a new gaussian. It is also true that a down-scaled gaussian is a gaussian and will thus create a gaussian if convolved with another gaussian. If the down-scaling–convolution procedure is repeated a number of times and then scaled back to the original size it will result in a new and normalized gaussian with $C_i = \sum_{n=1}^{i} C_n \prod_{j=1}^{n} \Delta_j^2$ were Δ is the downsampling factor used.

The fact that each iteration can be seen as an convolution of the previous means that the total operation working on data d can be written as $d * a_1 * a_2 * \cdots * a_i$ or simply $d * a_n$ by using the convolution associativity and the fact that the kernels are gaussian. For continuous data this means that an iteration of MANA is equal to the generation of a new scale of $s \cdot c$ and c using the gaussian kernel a_n, but due to the fact that real world data is discrete the relation must be seen as an approximation. The flowchart in figure 2 is thus approximately equivalent to figure 1.

3.2. Scale Weighting

Once a new scale is created through an iteration of MANA the result is used to update the estimate $\tilde{s}$. Since the jump between scales can be quite large, depending on the kernel and downsampling factor used, it is necessary to combine information from more than one scale. Here the combination is done using a weighted average based on a smoothing factor β. In this section a convolution with a_i will denote the scale generated by iteration i.

In this paper a simple weight function based on the latest $c * a_i$ and previous $c * a_{i-1}$ iterations is used. This is mainly to reduce memory usage. It is however possible to create a large number of weight functions depending on how fine and coarse scales should be

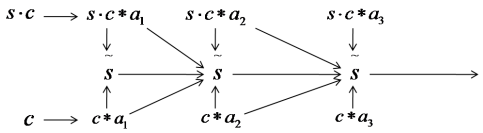

Fig. 2: The equivalence to figure 1 using the results of section 3.1.

prioritized. If more scales are included it is also possible to base the weights on information such as local trends.

The scale weighting is calculated using normalized scale certainties. The normalization is performed by dividing the certainties by the maximum value of the corresponding kernel for that iteration. This operation makes the certainties equal to that calculated by a kernel with 1 as maximum and the results become comparable from an uncertainty/density perspective. This type of operation is explained in [5] where gaussian smoothing is used to build a density scale space of the certainty in the same manner as here.

After a new iteration a point in $\tilde{s}$ is updated if the following inequities hold true: $c*a_{i-1}/max(a_{i-1}) < \beta$ and $c*a_i/max(a_i) \geq \beta$. The first expression excludes points where $\tilde{s}$ has been set in a previous iteration, one exception being the very first iteration. The second expression excludes points where the certainty is too low on the coarse scale. A larger β will cause the estimation to be based on coarser scales and thus give smoother and less local estimates. The value of the new point is a linear combination of the two current scales using eq. 3. The weight w is calculated using eq. 4 and is bound to $]0, 1]$ since the denominator is larger or equal to the nominator for all points satisfying the update inequalities. If $c * a_i/max(a_i) = \beta$ only the coarse scale will be used. As $c * a_i/max(a_i)$ grow larger the weigh shifts towards the finer scale. The coarse scale is also used if the finer scale does not contain any information since $c * a_{i-1}/max(a_{i-1}) = 0$ in eq. 3.

$$\tilde{s} = \frac{(1-w)\cdot(s\cdot c * a_{i-1}) + w\cdot(s\cdot c * a_i)}{(1-w)\cdot(c * a_{i-1}) + w\cdot(c * a_i)} \tag{3}$$

$$w = \frac{\beta - c * a_{i-1}/max(a_{i-1})}{c * a_i/max(a_i) - c * a_{i-1}/max(a_{i-1})} \tag{4}$$

$$\text{were } c * a_i/max(a_i) \geq \beta \text{ and } c * a_{i-1}/max(a_{i-1}) < \beta$$

The parameters of MANA effect the result of the final estimation. σ defines the first scale and in combination with Δ how fast the locality of the scales change. These parameters are both important for the result of each scale and the final result when combined with β. The certainty estimate used for the scale weighing can roughly be interpreted as an approximation of density estimates using binary spherically symmetric filters were the radii of the filters are equal to σ_i. This is motivated by the fact that $a_i/max(a_i)$ will be close to 1 within the radios of σ_i and then decline fast. Thus a response of $c * a_i/max(a_i)$ can be interpreted as an estimate of the number of samples, or certainty density, within the sphere spanned by σ_i. β becomes the minimum number of samples in the sphere needed in order to incorporate a scale into the final estimation.

4. RESULTS

The intensity correction was performed on 50 whole-body datasets from a 1.5 T Philips Achieva MR-scanner (Philips Medical Systems, Best, The Netherlands). Dual echo Dixon volumes [6] was acquired using the quadrature body coil. The voxel volume was 41.3 mm^3.

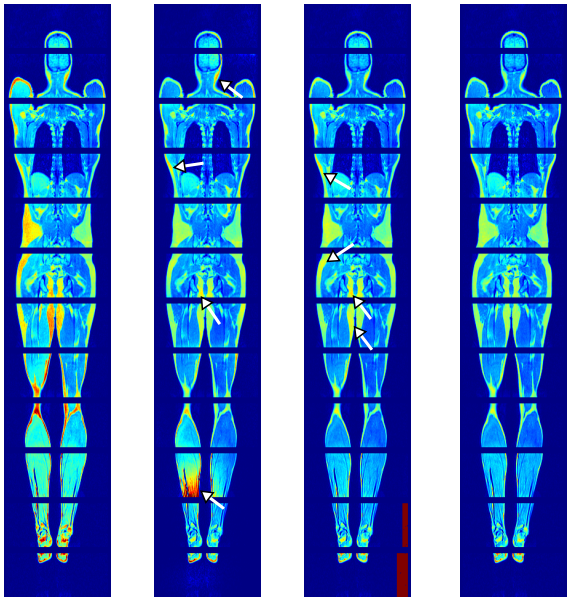

(a) (b) (c) (d)

Fig. 3: Original $fat + water$ image (a), intensity correction using second degree polynomial basis function (b), intensity correction using NA with a $\sigma = 20$ (c), intensity correction using MANA (d). To better visualize the result all images are presented in pseudo color.

The inverse gradient method [7] was used for the phase sensitive reconstruction required to create fat–water images.

Voxels containing at least 90% fat signal were classified as fat voxels and used for the bias field estimation. For the estimation using MANA the parameters were set to $\Delta = 2$, $\sigma = 2$ and $\beta = 27$. For comparison the bias field was also estimated using a least square fitting onto a set of second degree polynomial basis functions and NA with a gaussian kernel $\sigma = 20$.

The inhomogeneity correction was performed in Matlab (Mathworks). Convolutions were performed using multiple threads and separable kernels. The interpolation was done tri-linearly and multi threaded. All calculations were performed on a workstation with 2 quad core Intel Xeon X5560 CPUs at 2.8 GHz. For whole body bias field estimations the averaged computation times were 7.21 ± 1.00 sec using MANA, 5.89 ± 0.64 sec using NA and 0.75 ± 0.14 sec for the polynomial fitting.

A two-way (method/patient) ANOVA with Tukey-Kramer *post-hoc* analysis of 50 intensity corrected whole body fat volumes showed that the methods resulted in systematic differences in measured fat volume($p < 0.01$). Fat intensity histograms using only pure fat voxels were created for all whole body datasets and the full width half maximum (FWHM) was calculated. This resulted in a mean FWHM of 0.34 ± 0.04 before correction, 0.18 ± 0.02 using polynomial fitting, 0.18 ± 0.02 using NA and 0.11 ± 0.01 using MANA. The FWHM values was subjected to an ANOVA with Tukey-Kramer *post-hoc* analysis which resulted in a significant difference between MANA and the other methods ($p < 0.01$).

The results from the intensity inhomogeneity correction using the three methods can be seen in figures 3 and 4. The polynomial based bias field correction shown in 3b failed when the pure fat voxels become sparse and unevenly distributed. The polynomial basis fitting resulted in unrealistic values, i.e. the calf. The differences

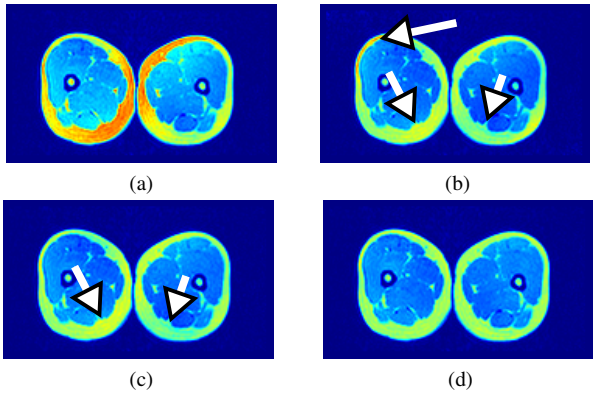

(a) (b) (c) (d)

Fig. 4: Original $fat + water$ image (a), intensity correction using second degree polynomial basis function (b), intensity correction using NA with a $\sigma = 20$ (c), intensity correction using MANA (d). To better visualize the result all images are presented in pseudo color.

between NA and MANA figures 3c, 3d, 4c, 4d were more subtle and are pointed out by arrows. Figure 5 illustrates how σ effected the inhomogeneity correction using NA, and how a too small filter introduced artifacts in low fat areas.

Figure 6 shows intensity histograms of the fat and water volume before and after intensity correction using the three methods. These figures show that the intensities became more homogeneous as the bimodal nature of the histograms became more apparent. When creating the histograms a mask was applied to remove low SNR voxels (i. e. areas outside the body and in the lungs). The mask was created by thresholding the $fat + water$ volume.

5. DISCUSSION

The polynomial fitting was significantly faster compared to NA and MANA but lacked robustness when the pure fat voxels became sparse and unevenly distributed throughout the volume. This source of error is avoided in NA and MANA since they rely on averages and will thus always generate results within the intensity range of the classified fat voxels.

The main drawback of NA is that the result is highly dependent on the filter kernel. A small kernel is preferable since it will capture fast changes in intensity, but a small filter will also increase the risk of producing artifacts. Two of these artifacts are pointed out in figure 5b. The first one occur when the distance to the closest certain sample become too large and the field can not be estimated. The second one is more subtle and arises when two clusters with different intensities are located in such a way that the filter response quickly changes from one to the other. The only way of avoiding these sources of errors is to use a larger filter. Thus the optimal kernel for a given volume changes with the distribution of fat. A safe choice of kernel will most likely not capture the bias field. This will not occur with MANA, even though MANA uses a much smaller kernel. MANA will use fine scales in fatty areas and thus capture the changes. Outside the fatty areas MANA will gradually shift to coarser scales when the distance from the fat cluster increases.

Since MANA is flexible the filter can be chosen to match the data trends and not only the distribution of samples. In this paper σ was set to 2, or 7 mm, to match the intensity variations caused by the coil sensitivity. β was set to 27 so the majority of the voxels in the local volume had to be pure fat in order for the finest scale to be used. The

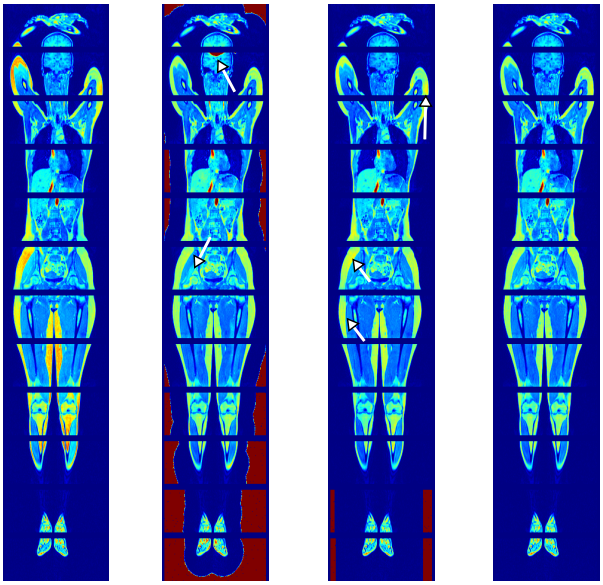

(a) (b) (c) (d)

Fig. 5: Original $fat + water$ image (a), intensity correction using NA with a $\sigma = 3.5$ kernel (b), intensity correction using NA with a $\sigma = 20$(c), intensity correction using MANA (d). The images are presented in pseudo color.

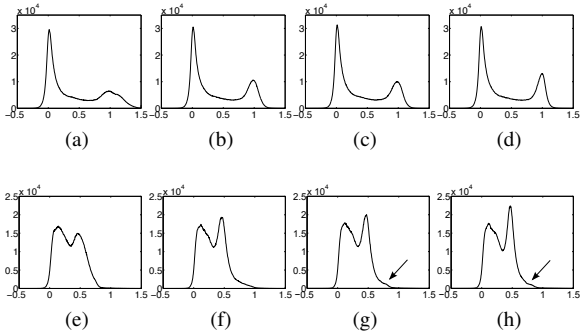

(a) (b) (c) (d)

(e) (f) (g) (h)

Fig. 6: Intensity histograms of the fat (above) and water (below) volumes. The histograms are based on the dataset in figure 4. Before (a/e), after correction using polynomial basis functions (b/f), using NA $\sigma = 20$ (c/g) and MANA (d/h). The water tissue peak at 0.5 become more distinct after correction and is most distinct for MANA. After the correction a small 'bump' can be seen (arrows), this feature is mainly built up by the liver and is completely obscured in (e). The FWHM of the fat peaks of a-d are 0.46, 0.23, 0.24 and 0.17

criterion is based on the fact that local information is needed in order to allow fast changes, otherwise artifacts may be created in sparse areas. Δ is a trade of between locality, computationally complexity and robustness. A large value will lower the number of calculations but increase the differences of the scales and lead to aliasing errors, which can escalate through the iterations if it is not matched to σ. $\Delta = 2$ and a $\sigma = 2$ avoids aliasing errors while providing fair computational complexity and locality scaling.

The computational efficiency of MANA is shown by the fact that it manages to produce a sample density based adaptive estimation in about the same time as a single NA operation. This is accomplished by using a smaller filter kernel applied on several resolutions of the data. Since both the convolution and interpolation operations are easy to parallelize MANA is suiting for large dataset and modern computers.

The histograms of figure 6 and the pure fat voxel FWHM reduction shows that the intensities are more homogeneous after intensity correction. This can be confirmed visually in figures 3 and 4, and by studying the FWHM changes of the fat voxles. The improvement of the water volume is interesting since the water voxel intensities are not used for the normalization itself. It can also be seen that MANA produce more homogeneous intensities when the broadness of the water peak at 0.5 is compared to the two other methods. The water homogenization combined with the reduction in FWHM of pure fat voxels indicate that MANA gives better results independent of location. This property of the bias field estimate allows quantification of fat in low certainty areas like thin structures and diffuse fat/water tissue such as brown adipose tissue and possibly also liver steatosis.

6. ACKNOWLEDGMENTS

Financial support from the Swedish research council (VR/M 2007-2884), the Swedish eScience Research Center (SeRC) and the Linköping University Hospital Research Foundations are gratefully acknowledged. We thank research nurses Annika Hall and Johan Kihlberg at the Center for Medical Image science and Visualization (CMIV) for assistance with data collection. Ethics permit was granted by the local ethics committee.

7. REFERENCES

[1] O. D. Leinhard, A. Johansson, J. Rydell, M. Borga, and P. Lundberg, "Intensity inhomogeneity correction in two point Dixon imaging," in *Proceedings of ISMRM'08*, Toronto, Canada, May 2008, ISMRM, vol. 16, p. 1519.

[2] O. Dahlqvist Leinhard, A. Johansson, J. Rydell, Ö. Smedby, F. Nyström, P. Lundberg, and M. Borga, "Quantitative abdominal fat estimation using MRI," in *19th International Conference on Pattern Recognition (ICPR)*, Tampa, FL, USA, December 2008.

[3] H. Knutsson and C-F. Westin, "Normalized and differential convolution: Methods for interpolation and filtering of incomplete and uncertain data," in *CVPR*, June 1993, pp. 515–523.

[4] Tuan Q. Pham and Lucas J. van Vliet, "Normalized averaging using adaptive applicability functions with applications in image reconstruction from sparsely and randomly sampled data," in *Image Analysis*, pp. 25–34. Springer Berlin / Heidelberg, 2003, ISSN 0302-9743 (Print) 1611-3349 (Online).

[5] Tuan Q. Pham, Lucas J. van Vliet, and Klamer Schutte, "Robust fusion of irregularly sampled data using adaptive normalized convolution," *EURASIP*, pp. 1–12, 2006.

[6] WT Dixon, "Simple proton spectroscopic imaging," *Radiology*, pp. 189–94, 1984.

[7] J. Rydell, H. Knutsson, J. Pettersson, A. Johansson, G. Farnebäck, O. Dahlqvist, P. Lundberg, F. Nyström, and M. Borga, "Phase sensitive reconstruction for water/fat separation in MR imaging using inverse gradient," in *MICCAI'07*, Brisbane, Australia, October 2007.